Bollettino di Geofisica Teorica ed Applicata Vol. 55, n. 4, pp. 699-716; December 2014
DOI 10.4430/bgta0129

3D analogue modelling of transtensional pull-apart basins: comparison with the Cinarcik basin, Sea of Marmara, Turkey

M. Sugan[1], J.E.L. Wu[2, 3] and K. McClay[2]

[1] *Istituto Nazionale di Oceanografia e di Geofisica Sperimentale (OGS), Udine, Italy*
[2] *Fault Dynamics Research Group, Royal Holloway, University of London, Egham, U.K.*
[3] *presently at: Department of Geosciences, National Taiwan University, Taipei, Taiwan*

(Received: January 30, 2014; accepted: April 29, 2014)

ABSTRACT Scaled 3D sandbox models have been used to investigate the 3D geometry and evolution of transtensional pull-apart basins. In this paper two representative analogue models were constructed to simulate the evolution of a 5° transtensional pull-apart basin formed above an underlapping, 45° strike-slip releasing bend basement stepover. Model 1 had 1:1 relative motion between opposing plates whereas Model 2 had 2:1 relative plate motion. In both experiments, a rhomboidal pull-apart basin developed with one central depocentre that was bounded by en-echelon basin margin faults. The early stages of basin evolution were characterised by basin subsidence and the nucleation of en-echelon normal faults. In the latter stages strike-slip occurred along the en-echelon normal faults, a cross-basin strike-slip fault formed and incremental basin subsidence decreased. Model 1 developed a symmetric basin whereas Model 2 developed a weakly asymmetric basin that had very active basin margin faults above the faster moving plate and a segmented cross-basin strike-slip fault system. The models were compared to the Cinarcik basin, Sea of Marmara. Both the analogue models and the natural prototype were characterised by basin margins bounded on one side by a simple, steeply-dipping normal fault and on the other side by an en-echelon array of steeply-dipping normal faults. The Model 1 showed similarities to the central and eastern part of the Cinarcik basin.

Key words: analogue modelling, pull-apart basins, transtension, en-echelon faults, Cinarcik basin, Sea of Marmara.

1. Introduction

In this study, the 3D geometry and evolution of a pull-apart basin in a transtensional regime was investigated using scaled sandbox models. Previous analogue models of pull-apart basins have proved to be a useful tool for simulating pull-apart basin geometries and evolution in both pure strike-slip (Hempton and Neher, 1986; Richard *et al.*, 1995; Dooley and McClay, 1997; Rahe *et al.*, 1998; Sims *et al.*, 1999) and in transtensional regimes (Dooley *et al.*, 2004; Wu *et al.*, 2009). These analogue model experiments simulate deformation in the sedimentary cover above a pre-defined underlying basement fault system.

The analogue modelling experiments presented here were designed to simulate the evolution

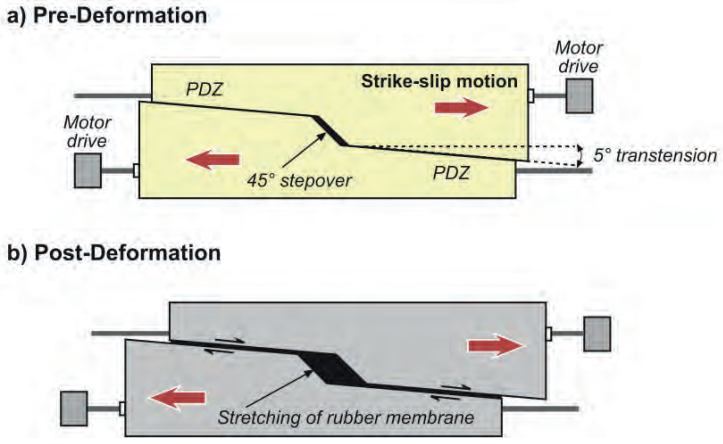

Fig. 1 - Plan view of the baseplate geometry used for the experiments. Transtension was produced by displacement of the plates 5° oblique to the principal displacement zones (PDZs). The stepover was underlain by a thin rubber membrane that stretched as the plates were displaced.

of a pull-apart basin above a basement stepover of a left-stepping, underlapping releasing bend in 5° dextral transtension (Fig. 1). In particular these models were designed to simulate the evolution of structures formed over the principal displacement zones (PDZs) and the basement stepover. In the models a single horizontal basal decollement was used in order to clearly demonstrate the link between displacement along the PDZs and the structural evolution of the cover sequence. Crustal complexities or mantle discontinuities were not incorporated and this should be taken in to account when comparing the analogue model experiments with natural prototypes characterized by complex geodynamic settings.

These experiments build upon previous studies of transtensional pull-apart basins (e.g., Dooley *et al.*, 2004; Wu *et al.*, 2009) by using a new basement stepover geometry designed to be similar to that proposed by Armijo *et al.* (2002) for the Cinarcik basin, in the Sea of Marmara, Turkey. The comparison between the analogue modelling experiments and the natural system could contribute to the further understanding of the relation between the evolution of the Cinarcik basin and the North Anatolian Fault (NAF) in the Sea of Marmara (e.g., Şengör *et al.*, 1985). The experiments also tested the effects of differential relative plate motion, a kinematic boundary condition of the Marmara Sea for the past 5 Ma that is indicated by Marmara sea geodesy and geological studies (e.g., Armijo *et al.*,1999; McClusky *et al.*, 2003). The pull-apart basin experiments presented here used transtensional plate motions that specifically allow comparison with the Sea of Marmara, which is located in a transition zone between a pure dextral strike-slip regime to the east of Izmit Gulf and a primarily extensional system to the west, in the Aegean Sea [Armijo *et al.* (1999) and references therein].

2. Analogue model procedure

The analogue model experiments described in this paper were designed to simulate the evolution of a pull-apart basin in a dextral transtensional regime (Fig. 1). The experiments were performed using baseplates with a 45° underlapping releasing bend and a 10 cm stepover

geometry. Transtension was obtained by displacing the plates 5° oblique and divergent to the PDZs. The stepover was underlain by a thin rubber membrane that was glued beneath the plates to simulate mid-crustal stretching. The sandbox had unconstrained longitudinal margins and had dimensions of approximately 100x50x10 cm. In order to simulate the sedimentary cover above a basement-induced fault system, a 7.5 cm dry quartz sand layer was used. Dry quartz sand with 31° angle of internal friction and a negligible cohesive strength has been widely demonstrated to be a suitable modelling material for simulating the brittle deformation of sediments in the upper crust (e.g., Horsefield, 1977; McClay, 1990). The models have a scaling ratio of approximately 10^{-5} such that 1 cm in the model corresponded to ~1 km in nature. They were deformed without the addition of syn-kinematic sediments in order to allow continuous monitoring of the surface deformation.

During the experiments, the two baseplates were moved in opposite directions by stepper motors with an average velocity of $4x10^{-3}$ cm/s to a total horizontal displacement of 8 cm.

Two 5° transtensional experiments are described in this paper. Model 1 had a 1:1 relative plate motion whereas Model 2 had a 2:1 plate motion in order to test the effect of differential plate motions on the evolution of the fault system. Sequential digital photographs of the upper surface were taken every 1 mm of horizontal offset on the PDZs. Laser scans were taken after every 1 cm of horizontal offset on the PDZs.

3. Analogue model results

Fig. 2 shows the 2D plan view evolution of Model 1 with 5° transtension and a 1:1 relative plate motion. Photographs are complemented by laser scan images of the model surfaces depicting total subsidence and interpreted faults. After 1 cm of horizontal displacement, two oppositely-dipping normal faults had developed in the stepover region (Fig. 2b-1). Dextral Riedel-shear (R-shears) faults formed above the PDZs with a strike of 25° relative to the PDZs (Fig. 2b-1). At 2 cm displacement a rhomboidal proto-basin had formed in the stepover region that consisted of a central graben and external grabens (Fig. 2b-2). As the basin subsided, above the PDZs the R-shears continued to develop and lengthened, synthetic P-shears started to form, and *en-echelon* faults propagated at the margins of the basin (Fig. 2b-2). After 3 cm, the pull-apart basin was well-developed with one central depocentre (Fig. 2b-3), P-shears were clearly developed, linking the dextral R-shears above the PDZs. Between 4 and 5 cm of displacement the normal fault that bounded the southern basin margin began to accommodate significant strike slip displacement and overprinted the earlier normal faulting (Figs. 2b-4 and 2b-5). Above the PDZs, a narrow and elongate graben system formed from the linkage of anastamosing *en-echelon* fault segments (Figs. 2b-4 and 2b-5). After 6 cm of horizontal displacement new N-S oriented fault segments began to initiate within the pull-apart basin (Figs. 2b-6 and 2b-7).

Incremental basin subsidence (Fig. 3) was calculated by subtracting successive laser scans of the model surface. At each stage the maximum subsidence occurred within the central depocentre. Maximum incremental subsidence per 1 cm strike-slip displacement along the PDZs gradually increased to a maximum of 6.5 mm at 3 and 4 cm of strike-slip PDZ displacement (Figs. 3a to 3d). Incremental subsidence decreased conspicuously to ~4 mm at 5 and 6 cm of strike-slip PDZ displacement (Figs. 3e and 3f). The marked decrease in basin subsidence was

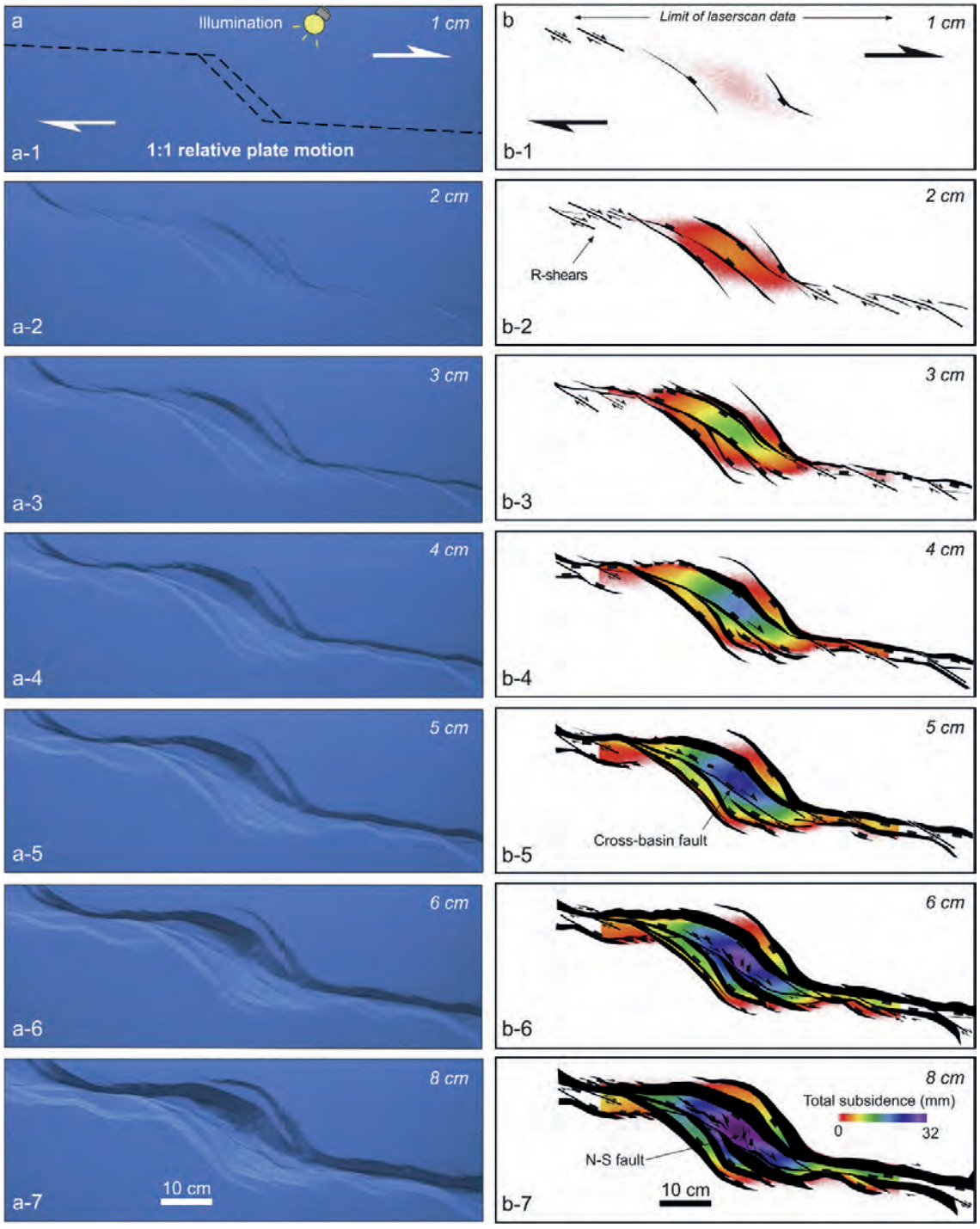

Fig. 2 - Plan view evolution of Model 1 with 5° transtension and 1:1 relative plate motion illustrated by: a) time-lapse overhead photography; b) laser scan data showing total depth of basin and interpreted faults.

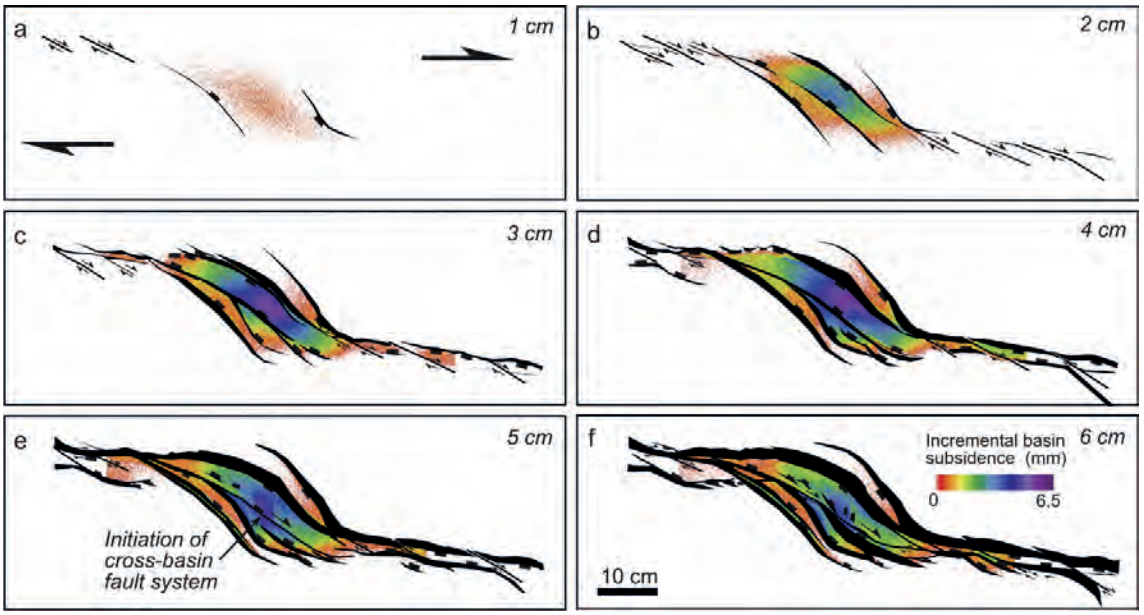

Fig. 3 - Incremental basin subsidence in Model 1 with 5° transtension and 1:1 relative plate motion for the first 6 cm of horizontal displacement along the PDZs. Incremental basin subsidence was calculated from successive laser scans and faults were interpreted from sequential photographs.

concurrent with the development of a major cross-basin strike-slip fault system (e.g., Figs. 3e and 3f), which linked the offset PDZs.

Fig. 4 shows the 2D plan view evolution of Model 2 with 5° transtension and a 2:1 relative plate motion. Here the experimental results are displayed such that the faster moving plate is at the bottom margin (i.e., south) with respect to the photographs. This orientation is maintained in subsequent figures to enable the later comparison to the NAF system, which has a present day faster-moving southern plate (McClusky *et al.*, 2003). Early basin evolution in Model 2 was characterised by a rhomboidal area of subsidence above the basement stepover (Figs. 4b-1 and 4b-2). After 1 cm of horizontal displacement, basin-bounding normal faults generated on the side with the faster moving plate (i.e., the lower left plate with respect to the photographs of Fig. 4b-1). As horizontal displacement continued, the normal faults lengthened and linked (Fig. 4b-2). Basin-bounding normal faults generate on the side with the slower moving plate (i.e., the upper right plate with respect to the photographs) and an asymmetric basin was formed in plan view (Fig. 4b-2). Dextral R-shear faults formed above the PDZs with a strike of 25° relative to the PDZs (Fig. 4b-2). As displacement along the PDZs increased, basin margin faults on the side with the faster moving plate had conspicuously higher displacements than on the opposite, slower-moving side of the model basin. A cross-basin strike-slip fault system began to form at 4 cm of horizontal displacement on the PDZs (Fig. 4b-4). The cross-basin fault system consisted of a number of segmented, dextral strike-slip segments that nucleated and linked across the basin floor (Figs. 4b-4 to 4b-7). Incremental basin subsidence patterns for Model 2 (Fig. 5) show that basin subsidence was highest at the basin centre. The basin was weakly asymmetric and had higher subsidence and fault displacements on the side with the faster moving plate in the early stage of formation.

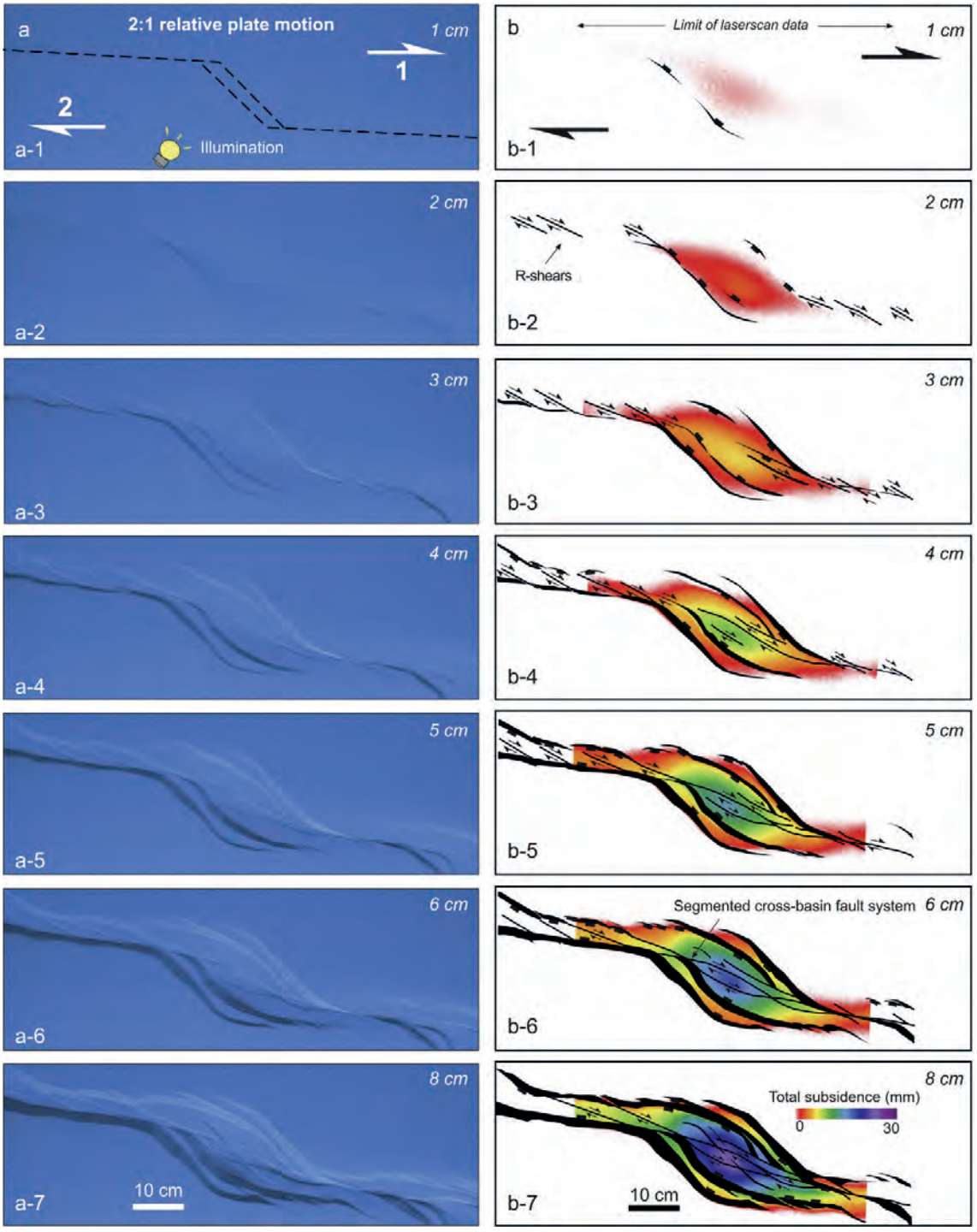

Fig. 4 - Plan view evolution of Model 2 with 5° transtension and 2:1 relative plate motion illustrated by: a) time-lapse overhead photography; b) laser scan data showing total depth of basin and interpreted faults.

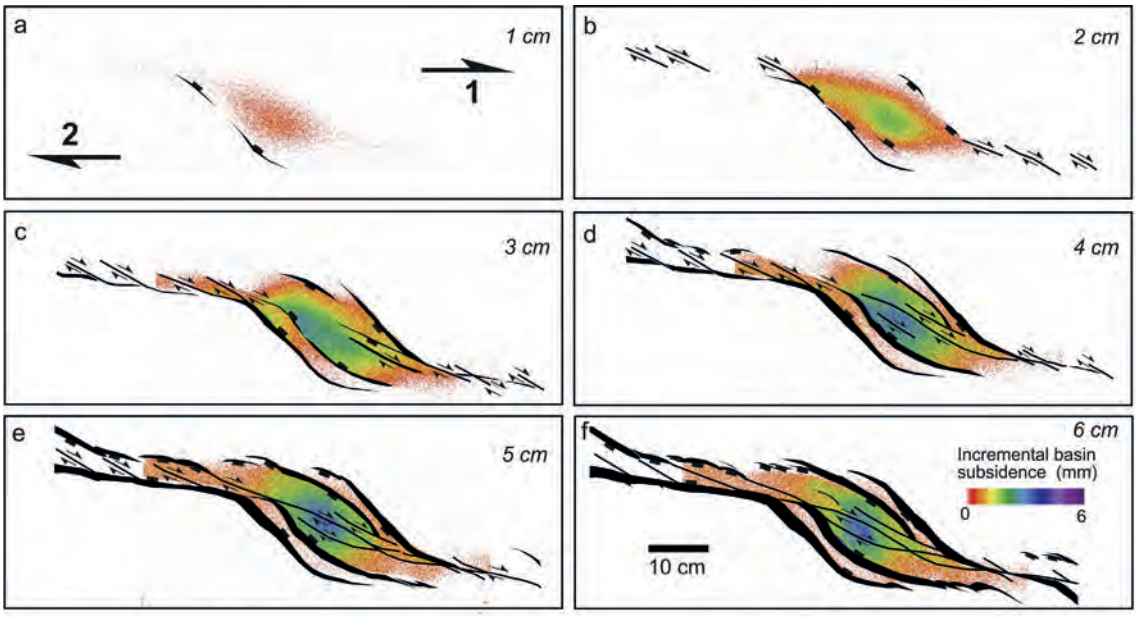

Fig. 5 - Incremental basin subsidence in Model 2 with 5° transtension and 2:1 relative plate motion for the first 6 cm of horizontal displacement along the PDZs. Incremental basin subsidence was calculated from successive laser scans and faults were interpreted from sequential photographs.

4. Discussion

4.1. Comparison of analogue Model 1 and 2 geometries

Models 1 and 2 (Figs. 2 and 4) both generated rhomboidal pull-apart basins. These basins were characterised by a single depocentre and basin margins with half-graben geometries. Above the offset PDZs, a distinct, narrow in-line graben system was formed and segmented, en-echelon normal faults formed where the basin margin faults linked to the offset PDZs. Similar features were formed in analogue models of transtensional pull-apart basins (Dooley and McClay, 1997; Rahe *et al*., 1998; Wu *et al*., 2009). Both models developed a cross-basin strike-slip fault system that linked the offset PDZs (e.g., Zhang *et al*., 1989; Dooley and McClay, 1997). In Model 1 a decrease in incremental subsidence occurred coeval with the development of the cross-basin strike-slip fault system.

Model 1, with 1:1 relative plate motions, produced a relatively symmetric basin (Fig. 2). In contrast Model 2, with 2:1 differential plate motions, produced an asymmetric model basin that was particularly conspicuous from its initial incremental basin subsidence patterns (Figs. 5a to 5c). The basin asymmetry appeared to be the result of the higher fault activities above the faster-moving plate (Figs. 4b-1 and 4b-2). The faults above the faster-moving southern plate in Model 2 formed first and hard-linked to form long fault traces (Fig. 4). In contrast the faults that formed above the slower moving northern plate in Model 2 were shorter and segmented. In published pure strike-slip analogue models, basin asymmetry due to differential plate motions occurred from the net movement of material away from the pinned, slower moving plate and towards the faster moving plate (Rahe *et al*., 1998). The model presented here show that basin asymmetry formed above differential plate motions is likely to be even more pronounced in transtensional settings, where there is greater net extension across the opposing basement blocks (e.g., Figs. 5a to 5c).

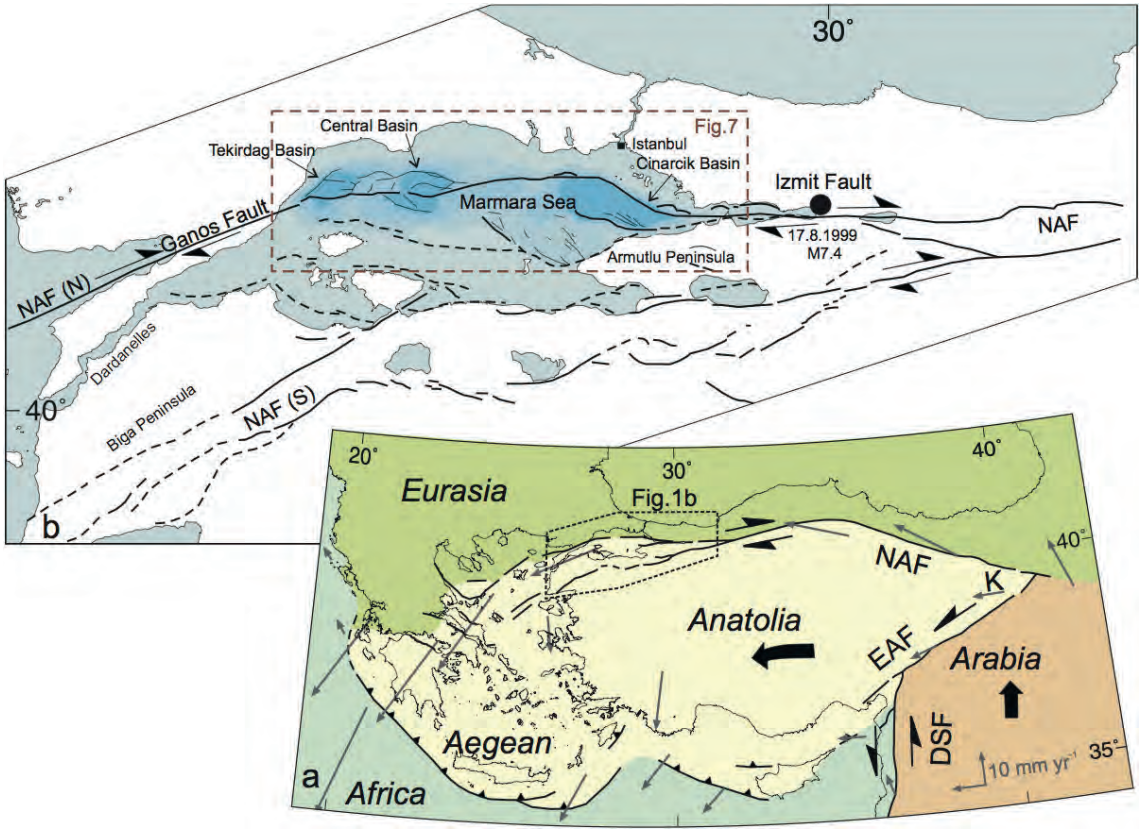

Fig. 6 - a) Regional tectonic setting of the Marmara Sea pull-apart system [modified from Armijo *et al*. (1999, 2002)]. b) Regional structural geometries of the Sea of Marmara region. Black dot shows the epicentre of the 1999.08.17 Izmit earthquake (*M* 7.4). Dotted box indicates details enlarged in Fig. 7. NAF = North Anatolian Fault; EAF = East Anatolian Fault; DSF = Dead Sea Fault; K = Karlinova triple junction. Grey vectors indicate the relative motions with respect to Eurasia derived from GPS (McClusky *et al*., 2003).

4.2. Comparison with the Cinarcik basin

In this section, the geological setting of the Cinarcik basin is briefly reviewed. Tectonic models for its formation are described. The analogue modelling results from this study are then compared to the plan view geometries, depocentre locations and cross-sections from Cinarcik basin.

4.2.1. Geological setting

The Cinarcik basin forms the easternmost seafloor depression at the Sea of Marmara (Fig. 6). Its evolution is related to the NAF, a right lateral transform fault that has splayed into two main branches in the Sea of Marmara region (Barka and Kadinsky-Cade, 1988; Barka, 1992; Yaltirak, 2002; Şengör *et al*., 2005). The NAF initiated in eastern Turkey between approximately 10 and 13 Ma and propagated westwards toward the Sea of Marmara (Şengör, 1979; Şengör *et al*., 1985; Hubert-Ferrari *et al*., 2002). On the basis of geological and present-day geodetic data (Armijo *et al*., 1999; McClusky *et al*., 2000) the northern branch of the NAF appears to transfer the most of the right-lateral strike slip motion across the Sea of Marmara [24±1 mm yr^{-1}: McClusky *et al*. (2003)].

Deep seismic reflection interpretations across the Sea of Marmara and Cinarcik basin show a number of faulted, tilted upper crustal blocks that form a negative flower structure (Laigle *et al*., 2008), whose faults detach above deep surface (Bécel *et al*., 2009, 2010). The Moho and the lower crust shallow towards the centre of the basin (Bécel *et al*., 2009).

The structures and geomorphology of the Cinarcik basin has been described by geological and geophysical data (e.g., Okay *et al*., 2000; Le Pichon *et al*., 2001; Armijo *et al*., 2002; Demirbağ *et al*., 2003; Gökaşan *et al*. 2003; Carton *et al*., 2007). In plan view the Cinarcik basin is approximately 50 km long, 20 km wide and has a rhomboid shape (Okay *et al*., 2000; Armijo *et al*., 2002; Kurt *el al*., 2013). The northern and southern margins of the eastern Cinarcik basin contain a series of down-to-the-basin normal faults (Okay *et al*., 2000; Armijo *et al*., 2002; Carton *et al*., 2007). The northern basin bounding fault has formed at an angle of about 30° to the E-W striking NAF and displays right-lateral offset of seafloor structures (Armijo *et al*., 2002). At the western end of the basin, thrusts and folds have been interpreted [Le Pichon *et al*. (2001) and reference therein]. The western margin of the basin is separated from the Central basin by a topographic high (i.e., Central High). The basin is predominantly flat-bottomed with maximum depth of 1270 m. The bathymetry of the northern margin dips towards the south at approximately 17° over a zone 3 km wide. In contrast the bathymetry of the southern margin has a more gentle dip of 7-10° towards the north over a zone 4-6 km wide (Okay *et al*., 2000).

The maximum syn-kinematic sedimentary thickness in the Cinarcik basin is estimated at 5-6 km (Carton *et al*., 2007). Sediment thickness maps reveal that the main depocentre has gradually migrated eastwards over time (Carton *et al*., 2007).

4.2.2. Tectonic models of the Cinarcik basin

Based on morphobathymetry, seismic reflection data and geological evidence, the Sea of Marmara has been interpreted as a series of active, or inactive, transtensional pull-apart basins (Barka and Kadinsky-Cade, 1988; Armijo *et al*., 1999, 2002; Rangin *et al*., 2004). 85 km of strike-slip displacement since 5 Ma has been interpreted between the Ganos and the Izmit faults that form the offset PDZs (Armijo *et al*., 1999). Within the greater pull-apart basin, shorter strike-slip fault segments link the Cinarcik, Central and Tekirdag sub-basins (Fig. 7a). At the Cinarcik basin the northern border fault has been strain partitioned into two fault strands, one of which has mainly strike-slip displacements and the other mainly normal displacements (Armijo *et al*., 2002). Reconstructions indicate that a significant amount of extension ~ 2 km has occurred at the northern border of the Cinarcik basin (Armijo *et al*., 2002).

A second model has interpreted a single throughgoing dextral strike-slip fault zone that has connected the Izmit and the Ganos faults (Fig. 7b) (e.g., Şengör *et al*., 1985; Aksu *et al*., 2000; Imren *et al*., 2001). The single strike-slip zone was supported by the predominance of pure strike-slip focal mechanisms at the Sea of Marmara, while en-echelon faults at the seafloor are interpreted as P-shears and antithetic Riedel shears of the fault zone (Le Pichon *et al*., 2001). Although a throughgoing strike-slip fault is interpreted along the northern border of the Cinarcik basin, it is acknowledged that the deformation at the Cinarcik basin is complex: the eastern basin is a zone of extension whereas the western basin is a zone of shortening and rotation (Le Pichon *et al*., 2001).

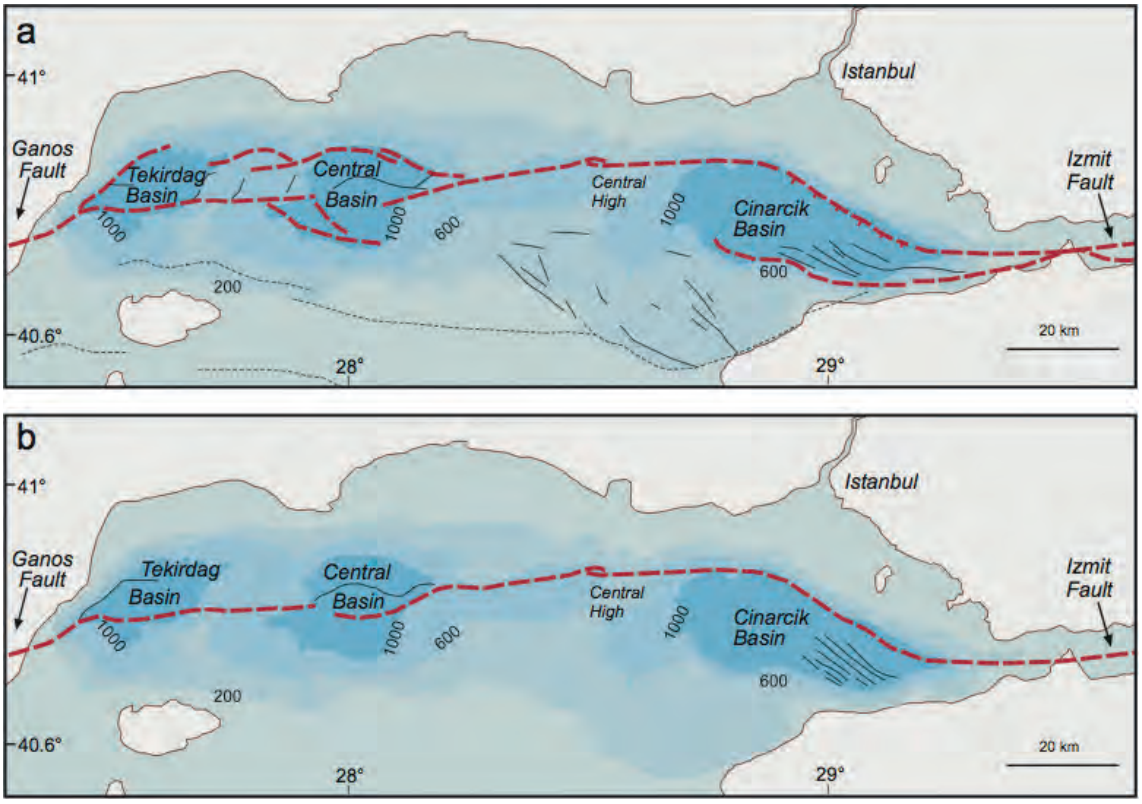

Fig. 7 - Schematic representation of the two main structural models of the NAF in the Marmara Sea fault zone, which connects the Izmit and Ganos faults: a) pull-apart basins [modified from Armijo *et al*. (2002)]; b) single thoroughgoing dextral strike-slip [modified from Le Pichon *et al*. (2001)]. Bathymetry is in metres.

Newer models have used deep seismic reflection profiles to interpret the Sea of Marmara as a series of tilted, asymmetric half grabens (Seeber *et al*., 2006, 2010; Laigle *et al*., 2008). In these models the Cinarcik basin formed at a bend in the NAF and basin subsidence was due to oblique slip on a steeply-dipping, non-vertical transform fault (Seeber *et al*., 2006, 2010). The Cinarcik basin depocentre moved with the Anatolian plate but was fixed relative to the opposing Eurasian plate, thereby generating a characteristic shingled, asymmetric wedge of syn-kinematic strata (Seeber *et al*., 2010).

In the next section the 'pull-apart basin' model for the Cinarcik basin is assessed by comparison of the analogue model geometries from this study to its published subsurface geometries.

4.2.3. Comparison of plan view geometries

A comparison of the plan view geometries of Model 1 and Model 2 and the Cinarcik basin is shown in Fig. 8. Both the model and natural prototype display a narrow, elongate full graben at the basin centre. However, in the analogue model the graben has developed at the basin centre (Fig. 8c) whereas at the Cinarcik basin the graben is offset towards the NE border fault (Figs. 8a and 8b). Both the model and natural prototype have relatively similar border faults that define an elongate rhomboidal basin. The Cinarcik basin, however, displays a much stronger

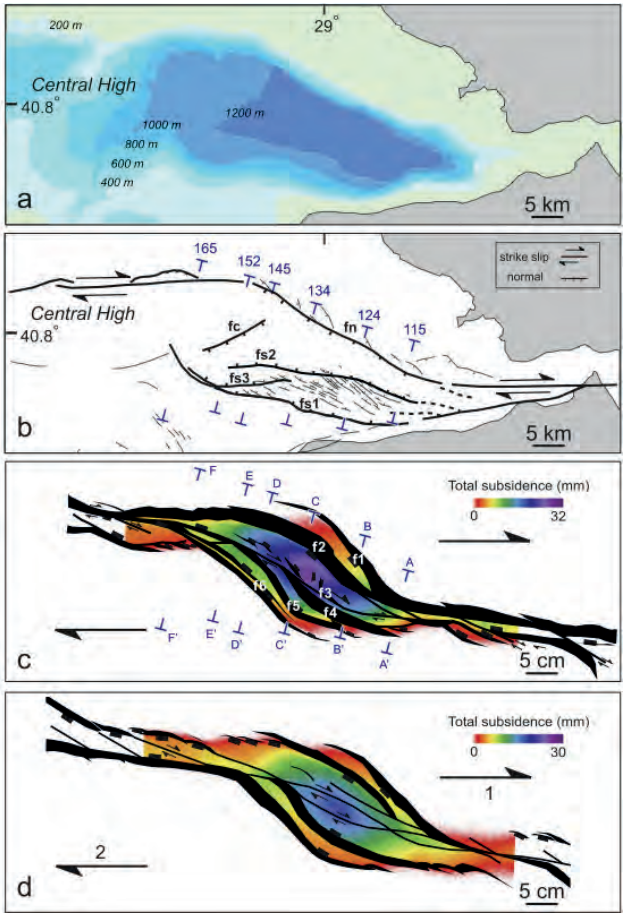

Fig. 8 - Comparison between maps of the Cinarcik basin and models 1 and 2: a) morphobathymetric map [modified from Armijo *et al*. (2002)]; b) map showing fault interpretation [modified from Armijo *et al*. (2002) and Carton *et al*. (2007)], also shown in Figs. 10a and 11a: fn = northern escarpment fault; fc = intra-basin fault; fs1 = southern margin fault; fs2 = inner boundary fault; fs3 = southwest bounding fault; in blue the location of seismic profiles shown in Figs. 10a and 11a; c) total subsidence and interpreted faults of Model 1 after 6 cm of horizontal displacement along the PDZs; in blue the location of cross sections shown in Figs. 10b and 11b; d) total subsidence and interpreted faults of Model 2 after 6 cm of horizontal displacement along the PDZs.

basin asymmetry than was developed in Model 1. The western Cinarcik basin is wider than the east side and has an elongated SW-NE trending depression that is bounded to the west by the 'Central High' structure (Figs. 8a and 8b). Folds and thrusts have been interpreted in the region from shallow seismic profiles [Le Pichon *et al*. (2001) and reference therein]: none of these features were developed in either Models 1 or 2 (Figs. 8c and 8d). If the Cinarcik basin is indeed a pull-apart basin, the asymmetry of its western half could possibly be explained by pre-existing basement geometries that were different to the idealized analogue model baseplate geometries (Fig. 1).

The Model 2 pull-apart basin with differential 2:1 relative plate motions developed a weakly asymmetric basin that had its main basin-bounding faults above the faster-moving 'southern plate' (Figs. 4 and 8d). In contrast, the Cinarcik basin has the opposite asymmetry:

its main basin-bounding fault is fixed to its slower-moving northern margin (e.g., Fig. 6b). This mismatch of basin margin fault geometries between analogue models and natural prototype suggests that the Cinarcik basin asymmetry is not likely explained by a transtensional pull-apart basin developed with differential relative plate motions. Instead, the model results suggest that 'transform-bend' basin models, which interpret oblique extensional slip along a single northern border fault system (e.g., Seeber *et al*., 2006, 2010), may better explain the border fault asymmetry of the Cinarcik basin than a pull-apart basin hypothesis. Transform-bend basin models are supported by the observation that many basins developed continental transform bends that have asymmetric plan view geometries (e.g., Mann 2007). Basins that develop asymmetry towards a transform fault have been explained by extension normal to the regional strike of the transform, concurrent with transform strike-slip motions (Ben-Avraham and Zoback, 1992).

4.2.4. Comparison of cross-sectional geometries

The fault geometries in the 3D isometric view in Fig. 9 were constructed by connecting surface deformation from Model 1 with known locations of basement discontinuities (i.e., the baseplate geometry). Although serial sections were not acquired to confirm the fault geometries, other similar analogue models constructed with sand display steeply-dipping, nearly planar fault geometries (e.g., Dooley and McClay, 1997; Rahe *et al*., 1998). The interpreted Model 1 fault geometries reveal en-echelon faulted pull-apart basin sidewalls that have a stepped topography (Fig. 9). Deformation above the PDZs was characterized by a shallow, narrow graben system (i.e., PDZ graben system), whose faults converged downwards to form negative flower structures.

In Figs. 10a and 11a the internal geometries of Cinarcik basin have been illustrated by six cross-sections interpreted from reflection seismic data by Carton *et al*. (2007). For comparison, six similarly-oriented sections are shown through Model 1 after 6 cm of horizontal displacement on the PDZs (Figs. 10b and 11b). At the eastern Cinarcik basin (Fig. 10), both the model and natural prototype had a northern margin formed by a steeply-dipping normal fault splay and a southern margin formed by an array of steeply-dipping, synthetic normal faults. A 3D visualisation shows the geometric similarities in the basin margin faults, the position of an en-echelon margin fault system and the general morphology of both the eastern Cinarcik basin and of the model (Fig. 12).

On the basis of the pattern of the syn-kinematic sedimentary sequences imaged along the interpreted seismic profiles of Fig. 10 [modified from Carton *et al*. (2007)] we can recognize two evolutionary phases in the central portion of the Cinarcik basin (Fig. 10, profile 134): an initial phase where vertical motion was mainly accommodated by the northern side; and a later stage, when tectonics along the southern margin prevailed. Analysis of the laser scans from the Model 1 indicated a similar deformation pattern in plan view during the basin evolution (Fig. 3): as the horizontal displacement increased from 4 to 6 cm, the highest subsidence rate migrated from the northern margin toward the southern margin.

The western half of the Cinarcik basin is wider towards the west and is composed of a deep, flat-bottomed basin bounded by high-displacement normal faults (Fig. 11a). The northern margin is formed by a single, steeply-dipping normal fault with associated splays while the southern basin margin is shaped by an array of synthetic normal faults (Fig. 11a). A sag within

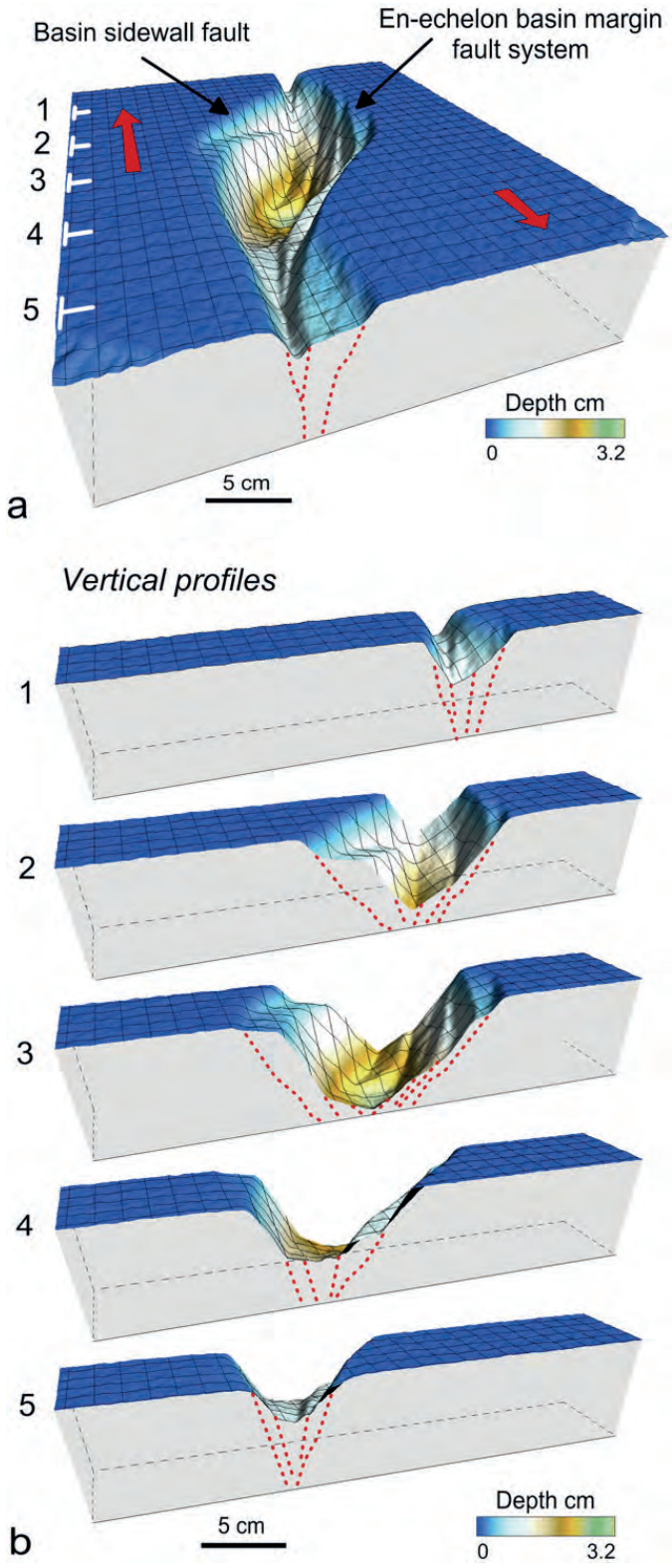

Fig. 9 - 3D visualisation and vertical profiles of transtensional pull-apart basin Model 1 after 6 cm of horizontal displacement along the PDZs. Dotted red lines = interpreted faults.

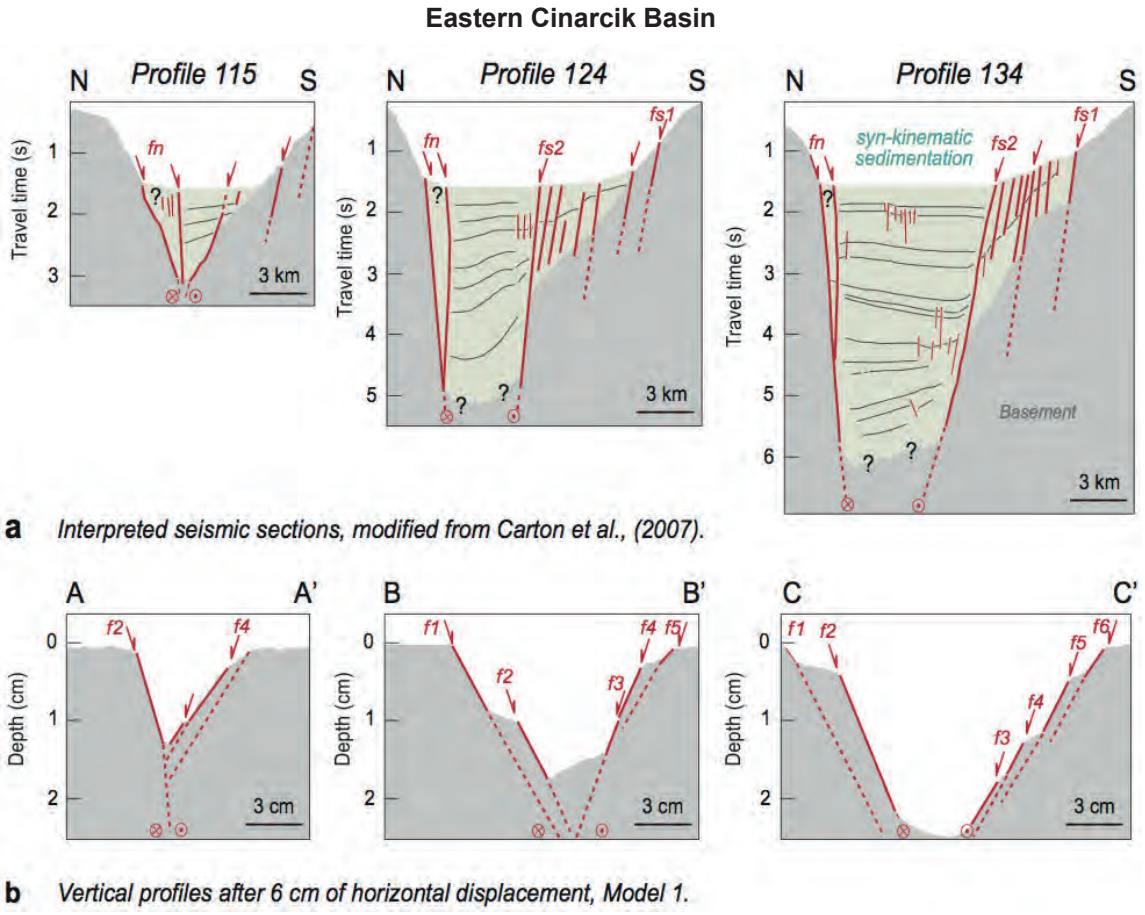

Fig. 10 - Comparison of interpreted seismic profiles (a) across the eastern Cinarcik basin [modified from Carton *et al.* (2007)] with three similarly-oriented profiles across Model 1 after 6 cm of horizontal displacement along the PDZs (b). Vertical exaggeration in (a) is about 4 for the seafloor, but it gradually decreases as it deepens within the sedimentary sequence, in (b) is about 4. Profile locations shown in Figs. 8b and 8c.

the syn-kinematic basin sediments in profiles 145 and 152 appears to have formed a discrete sub-basin (Fig. 11a) (Carton *et al.*, 2007). In contrast the western half of the Model 1 analogue model pull-apart basin became narrower and shallower towards the west and did not compare well with the western Cinarcik basin (Fig. 11b).

Deviation from the analogue model geometries at the western Cinarcik basin (Fig. 8a) may indicate the influence of pre-existing basement structures in the area (e.g., Okay *et al.*, 2000; Rangin *et al.*, 2004) and geodynamic settings that comprise upwarped lower crust and flower-style branching faults that cut the entire crust (Bécel *et al.*, 2009). The intra-basinal structural highs and sub-basins at the western Cinarcik basin, such as the Central High with over 400 m of bathymetric relief, could also be explained by pull-apart basin formation over a weak, ductile basal decollement (Sims *et al.*, 1999; Wu *et al.*, 2009). This is supported by seismic images of the deep structure to ~30 km depth below the Sea of Marmara that indicate tilted basement blocks developed over an intracrustal detachment (Laigle *et al.*, 2008; Bécel *et al.*, 2009, 2010). Alternatively these features have been interpreted as a series of thrust faults and associated folds due to oblique shortening (Le Pichon *et al.*, 2001).

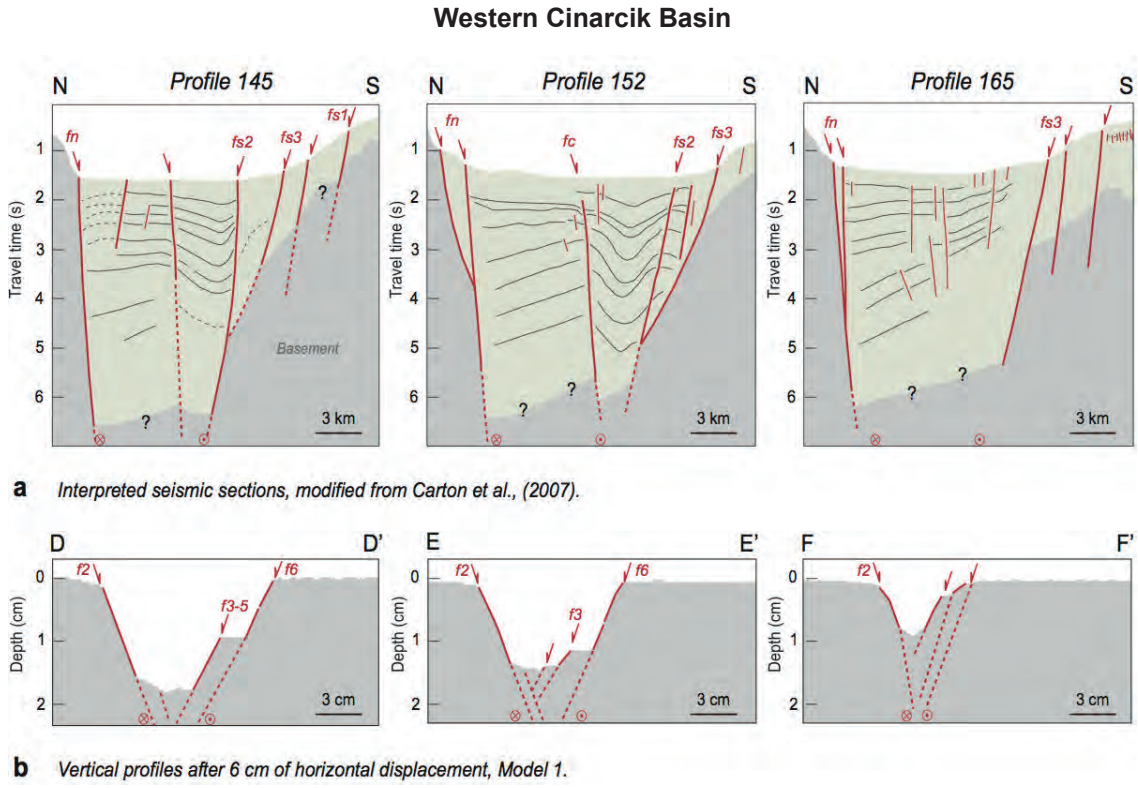

Fig. 11 - Comparison of interpreted seismic profiles (a) across the western Cinarcik basin [modified from Carton *et al*. (2007)] with three similarly-oriented profiles across Model 1 after 6 cm of horizontal displacement along the PDZs (b). Vertical exaggeration in (a) is about 4 for the seafloor, but it gradually decreases as it deepens within the sedimentary sequence, in (b) is about 4. Profile locations shown in Figs. 8b and 8c.

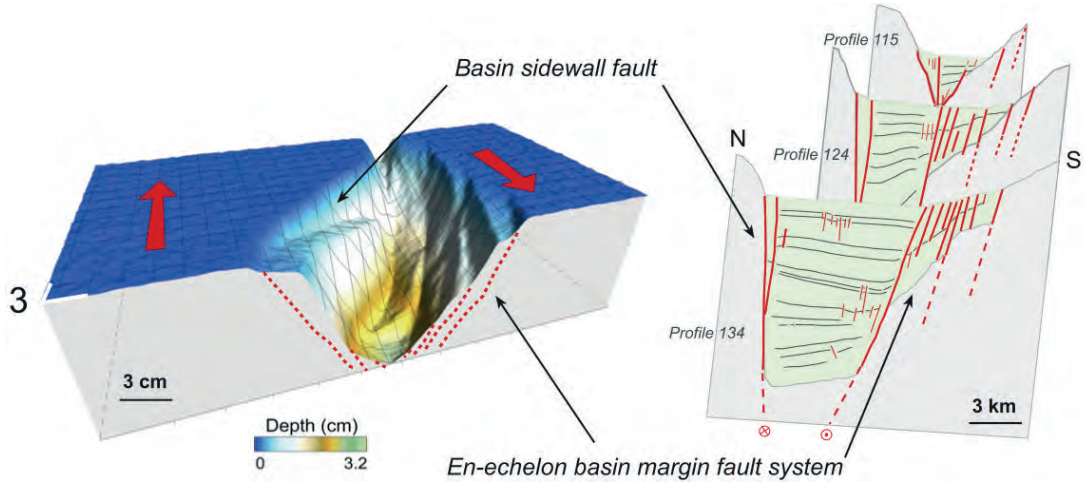

Fig. 12 - 3D view showing a comparison of the eastern part of the Cinarcik basin between the seismic profiles shown in Fig. 10a [modified from Carton *et al*. (2007)] and the Model 1 after 6 cm of horizontal displacement. Section 3 as in Fig. 9.

5. Conclusions

The two analogue models run with an underlapping 45° releasing stepover and 5° transtensional displacements developed an elongate rhomboidal pull-apart basin characterized by en-echelon faults at the basin margins and one central depocentre. A distinct narrow graben system developed over the PDZs. The model basins evolved in two main stages: an early stage characterised by basin subsidence and normal faulting and a second stage with predominant transcurrent movement characterised by the formation of a cross-basin strike-slip fault system. The model pull-apart basin with equal 1:1 relative plate motion was symmetric in plan view. In contrast, the model with differential 2:1 relative plate motion developed a mild asymmetric basin, characterised by a more active basin margin fault over the faster moving plate, and had a segmented cross-basin strike-slip fault.

Both the analogue models and the Cinarcik basin developed a narrow, elongate full graben in the basin centre. In the eastern half of the Cinarcik basin the analogue Model 1 roughly reproduced the northern border fault of the Cinarcik basin, an array of left-stepping en-echelon faults on the southern margin of the Cinarcik basin, and a dextral strike-slip fault above the PDZ. In cross-section both the eastern Cinarcik basin and the Model 1 had a northern margin formed by a steeply-dipping normal fault splay and a southern margin formed by an array of steeply-dipping, synthetic normal faults. The western Cinarcik basin is less similar to the analogue models in this study. The analogue model basin narrowed towards the west whereas the western Cinarcik basin is wider and is bounded by a NE-SW trending morphobathymetric high (i.e., Central High).

The results of the analogue models in this study suggest that an underlapping releasing basement stepover with 5° transtensional 1:1 displacement is sufficient to produce the approximate fault geometries and the shape of the Cinarcik basin, particularly in the eastern sector. This would support the applicability of a transtensional pull-apart structural model for the Sea of Marmara (e.g., Armijo *et al.*, 1999, 2002). However, differences between the asymmetric geometries of the Cinarcik basin and the analogue model pull-apart basin indicate that additional structural complexities exist. These may be related to pre-existing basement structures, a weak basal *decollement* layer, or extension normal to a transform fault bend.

Acknowledgments. The study was supported by EU Marie Curie Training Fellowship. Mike Craker is acknowledged for his assistance with building the modelling apparatus.

REFERENCES

Aksu A.E., Calon T.J., Hiscott R.N. and Yasar D.; 2000: *Anatomy of the North Anatolian fault zone in the Marmara Sea, Western Turkey: extensional basins above a continental transform*. GSA Today, **10**, 3-7.

Armijo R., Meyer B., Hubert A. and Barka A.; 1999: *Westward propagation of the North Anatolian fault into the northern Aegean: timing and kinematics*. Geology, **27**, 267-270.

Armijo R., Meyer B., Navarro S., King G. and Barka A.; 2002: *Asymmetric slip partitioning in the Sea of Marmara pull-apart: a clue to propagation processes of the North Anatolian Fault?* Terra Nova, **14**, 80-86.

Barka A.A.; 1992: *The North Anatolian fault zone*. Ann. Tectonics, **6**, 164–195.

Barka A.A. and Kadinsky-Cade K.; 1988: *Strike-slip fault geometry in Turkey and its influence on earthquake activity*. Tectonics, **7**, 663–684.

Bécel A., Laigle M., de Voogd B., Hirn A., Taymaz T., Galvé A., Shimamura H., Murai Y., Lépine J.C., Sapin M. and Ozalaybey S.; 2009: *Moho, crustal architecture and deep deformation under the North Marmara Trough, from the SEISMARMARA Leg 1 offshore-onshore reflection-refraction survey*. Tectonophysics, **467**, 1-21.

Bécel A., Laigle M., de Voogd B., Hirn A., Taymaz T., Yolsal-Cevikbilen S. and Shimamura H.; 2010: *North Marmara Trough architecture of basin infill, basement and faults, from PSDM reflection and OBS refraction seismics*. Tectonophysics, **490**, 1-14.

Ben-Avraham Z. and Zoback M.D.; 1992: *Transform-normal extension and asymmetric basins: an alternative to pull apart models*. Geology, **20**, 423-426.

Carton H., Singh S.C., Hirn A., Bazin S., de Voogd B., Vigner A., Ricolleau A., Cetin S., Ocakoglu N., Karakoc F. and Sevilgen V.; 2007: *Seismic imaging of the three-dimensional architecture of the Cınarcik Basin along the North Anatolian Fault*. J. Geophys. Res., **112**, b06101, doi: 10.1029/2006jb004548.

Demirbağ E., Rangin C., Le Pichon X. and Şengör A.M.C.; 2003: *Investigation of the tectonics of the Main Marmara Fault by means of deep-towed seismic data*. Tectonophysics, **361**, 1–19.

Dooley T. and McClay K.; 1997: *Analog modelling of strike-slip pull-apart basins*. AAPG Bulletin, **81**, 1804-1826.

Dooley T., Monastero F., Hall B., McClay K. and Whitehouse P.; 2004: *Scaled sandbox modelling of transtensional pull-apart basins: applications to the Coso geothermal system*. Geothermal Research Council Transactions, **28**, 637–641.

Gökaşan E., Ustaömer T., Gazioglu C., Yucel Z.Y., Öztürk K., Tur H., Ecevitoglu B. and Tok B.; 2003: *Morpho-tectonic evolution of the Marmara Sea inferred from multi-beam bathymetric and seismic data*. Geo-Marine Letters, **23**, 19-33.

Hempton M. and Neher K.; 1986: *Experimental fracture, strain and subsidence patterns over en-echelon strike-slip faults: implications for the structural evolution of pull-apart basins*, Journal of Structural Geology, **8**, 597–605.

Horsefield W.T.; 1977: *An experimental approach to basement-controlled faulting*, Geologie en Mijnbouw, **56**, 363–370.

Hubert-Ferrari A., Armijo R., King G., Meyer B. and Barka A.; 2002: *Morphology, displacement, and slip rates along the North Anatolian Fault, Turkey*. J. Geophys. Res., **107**, 2235, doi: 10.1029/2001JB000393.

Imren C., Le Pichon X., Rangin C., Demirbağ E., Ecevitoglu B. and Görür N.; 2001: *The North Anatolian Fault within the Sea of Marmara: a new interpretation based on multi-channel seismic and multibeam bathymetry data*, Earth and Planetary Science Letters, **186**, 143-158.

Kurt H., Sorlien C.C., Seeber L., Steckler M.S., Shillington D.J., Cifci G., Cormier M.-H., Dessa J.-X., Atgin O., Dondurur D., Demirbağ E., Okay S., Imren C., Gurcay S., and Carton H.; 2013: *Steady late Quaternary slip rate on the Cinarcik section of the North Anatolian fault near Istanbul, Turkey*. Geophysical Research Letters, **40**, 4555-4559, doi: 10.1002/grl.50882.

Laigle M., Bécel A., de Voogd B., Hirn A., Tayma T. and Ozalaybey S.; 2008: *the Members of the SEISMARMARA Leg 1. A first deep seismic survey in the Sea of Marmara: whole crust and deep basins*. Earth and Planetary Science Letters, **270**, 168-179.

Le Pichon X., Şengör A.M.C., Demirbağ E., Rangin C., Imren C., Armijo R., Görür N., Çağatay N., de Lepinay B.M., Meyer B., Saatchilar R. and Tok B.; 2001: *The active main Marmara fault*. Earth and Planetary Science Letters, **192**, 595-616.

Mann P.; 2007: *Global catalogue, classification and tectonic origins of restraining and releasing bends on active and ancient strike- slip fault systems*. In: Cunningham W.D. and Mann P. (eds), Tectonics of strike-slip restraining and releasing bends, Geological Society of London Special Publication 290, pp. 13–142.

McClay K.R.; 1990: *Deformation mechanisms in analogue models of extensional fault systems*. In: Knipe R. (ed), Deformation rheology and mechanics, Geological Society of London Special Publication 28, pp. 109-125.

McClusky S., Bassalanian S., Barka A., Demir C., Ergintav S., Georgiev I., Gurkan O., Hamburger M., Hurst K., Hans-Gert H.-G., Karstens K., Kekelidze G., King R., Kotzev V., Lenk O., Mahmoud S., Mishin A., Nadariya M., Ouzounis A., Paradissis D., Peter Y., Prilepin M., Relinger R., Sanli I., Seeger H., Tealeb A., Toksaz M.N. and Veis G.; 2000: *GPS constraints on plate kinematics and dynamics in the eastern Mediterranean and Caucasus*. Journal Geophys. Res., **105**, 5695-5719.

McClusky S., Reilinger R., Mahmoud S., Ben Sari D. and Tealeb A.; 2003: *GPS constraints on Africa (Nubia) and Arabia plate motions*. Geophys. J. Int., **155**, 126-138.

Okay A.I., Kaşhar-Özcan A., Imren C., Boztepe-Güney A., Demirbağ E. and Kuşçu I.; 2000: *Active faults and evolving strike-slip basins in the Marmara Sea, northwest Turkey: a multichannel seismic reflection study*. Tectonophysics, **321**, 189-218.

Rahe B., Ferrill D. and Morris A.; 1998: *Physical analog modelling of pull-apart basin evolution*. Tectonophysics, **285**, 21-40.

Rangin C., Le Pichon X., Demirbağ E. and Imren C.; 2004: *Strain localization in the Sea of Marmara: Propagation of the North Anatolian Fault in a now inactive pull-apart*. Tectonics, **23**, TC2014, doi: 10.1029/2002TC001437.

Richard P.D., Naylor M.A. and Koopman A.; 1995: *Experimental models of strike-slip tectonics*. Petroleum Geoscience, **1**, 71–80.

Seeber L., Cormier M.-H., McHugh C., Emre Ö., Polonia A. and Sorlien C.: 2006; *Rapid subsidence and sedimentation from oblique slip near a bend on the North Anatolian Transform in the Marmara Sea, Turkey*. Geology, **34**, 933–936.

Seeber L., Sorlien C., Steckler M. and Cormier M.-H.: 2010; *Continental transform basins: why are they asymmetric?* EOS. Transactions of the American Geophysical Union, **91**, 29-30.

Şengör A.M.C.; 1979: *The North Anatolian transform fault: its age, offset and tectonic significance*. J. Geol. Soc. London, **136**, 269-282.

Şengör A.M.C., Görür N. and Saroglu F.; 1985: *Strike-slip faulting and related basin formation in zones of tectonic escape: Turkey as a case study*. In: Biddle K.D. and Christie-Blick N. (eds), Strike-slip deformation, basin formation, and sedimentation, SEPM Spec. Publ.37, pp. 227-264.

Şengör A.M.C., Tuysuz O., Imren C., Sakinc M., Eyidogan H., Gorur N., Le Pichon X. and Rangin C.; 2005: *The North Anatolian Fault: a new look*. Ann. Rev Earth Planet Sci., **33**, 37-112.

Sims D., Ferrill D.A. and Stamatakos J.A.; 1999: *Role of a ductile decollement in the development of pull-apart basins: experimental results and natural examples*. Journal of Structural Geology, **21**, 533–554.

Wu J. E., McClay K., Whitehouse P. and Dooley T.; 2009: *4D analogue modelling of transtensional pull-apart basins*. Marine and Petroleum Geology, **26**, 1608–1623.

Yaltirak C.; 2002: *Tectonic evolution of the Marmara Sea and its surrounding*. Marine Geology, **190**, 493-529.

Zhang P., Burchfiel B.C., Chen S. and Deng Q.; 1989: *Extinction of pull-apart basins*. Geology, **17**, 814-817.

Corresponding author: Monica Sugan
Centro Ricerche Sismologiche, Istituto Nazionale di Oceanografia e di Geofisica Sperimentale (OGS),
via Treviso 55, 33100 Udine, Italy
Phone: +39 040 2140141; fax: +39 0432 522474; e-mail: msugan@inogs.it